4-2008

Continuous Cooling Transformation in Cast Duplex Stainless Steels CD3MN and CD3MWCuN

Yoon-Jun Kim
Iowa State University

L. Scott Chumbley
Iowa State University, chumbley@iastate.edu

Brian Gleeson
Iowa State University, bgleeson@iastate.edu

Continuous Cooling Transformation in Cast Duplex Stainless Steels CD3MN and CD3MWCuN

Abstract
The kinetics of brittle phase transformation in cast duplex stainless steels CD3MN and CD3MWCuN was investigated under continuous cooling conditions. Cooling rates slower than 5 °C/min. were obtained using a conventional tube furnace with a programable controller. In order to obtain controlled high cooling rates, a furnace equipped to grow crystals by means of the Bridgman method was used. Samples were soaked at 1100 °C for 30 min and cooled at different rates by changing the furnace position at various velocities. The velocity of the furnace movement was correlated to a continuous-cooling-temperature profile for the samples. Continuous-cooling-transformation (CCT) diagrams were constructed based on experimental observations through metallographic sample preparations and optical microscopy. These are compared to calculated diagrams derived from previously determined isothermal transformation diagrams. The theoretical calculations employed a modified Johnson-Mehl-Avrami (JMA) equation (or Avrami equation) under assumption of the additivity rule. Rockwell hardness tests were made to present the correlation between hardness change and the amount of brittle phases (determined by tint-etching to most likely be a combination of sigma + chi) after cooling.

Keywords
Engineering Design, Tribology, Corrosion and Coatings, Quality Control, Reliability, Safety and Risk

Disciplines
Metallurgy

Comments
This article is from *Journal of Materials Engineering and Performance* 17 (2008): 234-239, doi: 10.1007/s11665-007-9134-z. Posted with permission.

JMEPEG (2008) 17:234–239
DOI: 10.1007/s11665-007-9134-z

1059-9495/$19.00

Continuous Cooling Transformation in Cast Duplex Stainless Steels CD3MN and CD3MWCuN

Yoon-Jun Kim, L. Scott Chumbley, and Brian Gleeson

(Submitted April 24, 2007; in revised form May 10, 2007)

The kinetics of brittle phase transformation in cast duplex stainless steels CD3MN and CD3MWCuN was investigated under continuous cooling conditions. Cooling rates slower than 5 °C/min. were obtained using a conventional tube furnace with a programable controller. In order to obtain controlled high cooling rates, a furnace equipped to grow crystals by means of the Bridgman method was used. Samples were soaked at 1100 °C for 30 min and cooled at different rates by changing the furnace position at various velocities. The velocity of the furnace movement was correlated to a continuous-cooling-temperature profile for the samples. Continuous-cooling-transformation (CCT) diagrams were constructed based on experimental observations through metallographic sample preparations and optical microscopy. These are compared to calculated diagrams derived from previously determined isothermal transformation diagrams. The theoretical calculations employed a modified Johnson-Mehl-Avrami (JMA) equation (or Avrami equation) under assumption of the additivity rule. Rockwell hardness tests were made to present the correlation between hardness change and the amount of brittle phases (determined by tint-etching to most likely be a combination of sigma + chi) after cooling.

Keywords additivity rule, Bridgman method, cast duplex stainless steels, CCT diagrams, Rockwell hardness test

1. Introduction

Intermetallic precipitates such as σ, χ, and R phases, even in small amounts, are reported to degrade the favorable combination of toughness and corrosion resistance for which duplex stainless steels (DSS) are noted (Ref 1). Knowledge of the transformation behavior of intermetallic phases in DSS is of crucial importance in order to avoid a decrease in these properties. Time-temperature-transformation (TTT) diagrams provide fundamental information of transformation kinetics during isothermal conditions and play an important role as a guide to understanding phase transformation characteristics at a certain temperature of interest. TTT diagrams for a number of DSS with various compositions (mainly wrought alloys) have been constructed and published (Ref 1-4). However, a TTT diagram is somewhat less useful as a reference for industrial practices such as casting, hot rolling and welding, where the phase transformation can take place during cooling cycles associated with the process. Therefore, continuous-cooling-transformation (CCT) diagrams are critical. CCT diagrams typically have been experimentally determined at controlled cooling rates using thermal analysis such as dilatometry (Ref 4) as well as taking thermomechanical tests such as measurements of compression (Ref 5, 6), microhardness, (Ref 7) and strain (Ref 8).

While the Avrami equation (Ref 9) successfully describes isothermal transformation kinetics, it must be modified to accurately describe continuous cooling situations. Scheil (Ref 10) suggested the additivity rule, which assumes all nucleation takes place at the early stage of the reaction. This assumption is generally made in situations involving continuous cooling where heterogeneous nucleation occurs, and is often referred to as site saturation (Ref 11). Nucleation effects are negligible under this condition, so that growth is the predominate mechanism for such a reaction. Therefore, if the isothermal transformation behavior is known, a reliable mathematical model describing continuous cooling system can be derived by employing the additivity rule and manipulating the Avrami equation.

This article presents CCT diagrams for two cast DSS alloys, designated CD3MN (UNS J92205, ASTM A 890/A 890M 99 Grade 4A) and CD3MWCuN (UNS J93380, ASTM A 890/A 890M 99 Grade 6A). Exponents of the Avrami equation taken from experimentally determined TTT diagrams of both alloys (Ref 2, 3) were used to calculate CCT diagrams, which were then compared to experimental observations. Hardness measurements were carried out to correlate the effect of brittle phase precipitation on the mechanical properties of two DSS as a function of cooling rate and percent phase formation.

2. Mathematical CCT Model: A Modified Avrami Equation

Mathematically, transformation kinetics during continuous cooling can be considered as a series of steps under isothermal conditions that can be summed to as follows (Ref 11):

Yoon-Jun Kim, L. Scott Chumbley, and **Brian Gleeson,** Department of Materials Science and Engineering, Iowa State University, 2220 Hoover Hall, Ames, IA 50011-2300. Contact e-mail: chumbley@iastate.edu.

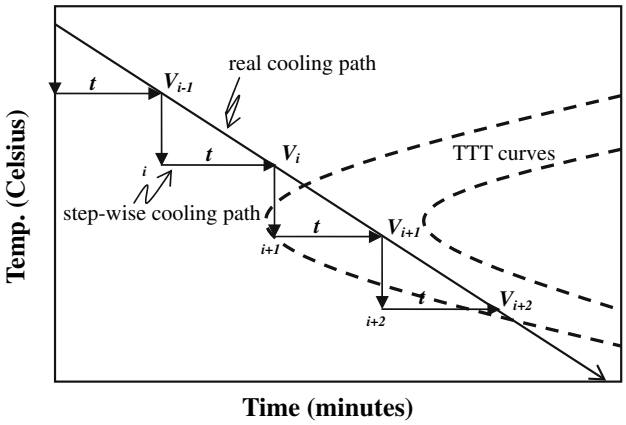

Fig. 1 Schematic description of a real cooling curve and a step-wise curve presented with TTT curves

$$\int_0^{t'} \frac{dt}{\tau} = \int_0^{T'} \frac{dT}{\tau\left(\frac{dT}{dt}\right)} = \int_0^{f'} \frac{df}{\tau\left(\frac{df}{dt}\right)} \quad \text{(Eq 1)}$$

where t is time, and τ is the time taken at a temperature T to achieve a specific amount (f) of product under isothermal conditions. In this additivity rule, τ, T and f are all obtained from a TTT diagram. The sufficient condition of this additive rule is that the nucleation rate is proportional to the growth rate, a so-called isokinetic condition. Nucleation site saturation is an alternate condition. If either condition is satisfied, Eq 1 equals to unity (Ref 11). Under this assumption Wilson et al. (Ref 12) modified the Avrami equation for a continuous cooling situation. Figure 1 shows schematically the methodology used. τ in Eq 1 is taken as the transformation starting time for a step i, and equals the time taken to produce the amount of V_{i-1} at the step i:

$$\tau_i = \left(\frac{\ln(1 - V_{i-1}/V_{ei})}{-k_i}\right)^{1/n_i} \quad \text{(Eq 2)}$$

where n_i and k_i are the exponents from the Avrami plot of the corresponding TTT diagram, V_{ei} is the equilibrium volume at the temperature i, and V_{i-1} is the volume transformed at the previous step i–1. Samples are presumably held for Δt, then quenched to the next step $i + 1$. The quantity Δt depends on the cooling rate and is fixed throughout the cooling process as long as the cooling rate stays the same. The modified Avrami equation for continuous cooling is thus given as follows:

$$f_i = \frac{V_i}{V_{ei}} = 1 - \exp\left[-k_i(\tau_i + \Delta t)^{n_i}\right] \quad \text{(Eq 3)}$$

At any temperature i, f, or V_i can be calculated and plotted, producing the desired continuous cooling curve.

It should be noted that experimentally it has been observed that the additivity rule can deviate from unity (Ref 13). To ensure that the assumption of unity is valid for the present study, extensive optical and SEM examination were carried out and the results are presented below.

3. Experiment

CD3MN and CD3MWCuN alloys were received in the form of keel blocks approximate size of $3 \times 4 \times 35$ cm. Their nominal compositions are given in Table 1. For slow cooling rates from 0.01 °C/min to 5 °C/min, blocks were sliced into small coupons about 4 mm thick by electrical discharge machining (EDM). The sliced coupons were encapsulated in quartz tubes filled with Ar gas in order to reduce oxidation during heat treatment at high temperature. Each sample was solution heat treated for 30 min at 1100 °C to homogenize the starting microstructure using a horizontal quartz tube furnace equipped with a temperature-controller, then cooled to room temperature at rates of 0.1, 0.5, 1, 2, and 5 °C/min. For cooling rates faster than this a directional solidification furnace used for producing Bridgman samples was employed. Sample rods with the dimensions 6.7 cm in length and 0.8 cm in diameter were prepared, with a K-type thermocouple wire inserted down the center. The furnace was set to 1100 °C, moved along the length of the sample at a fixed velocity, and the temperature profile monitored. Furnace velocities for this research were 0.100, 0.150, and 0.175 mm/s.

The manner in which quantitative measurements of precipitate phases were carried out are described in more detail elsewhere (Ref 2). Briefly, polished samples were subjected to electrolyte etching with 50 g NaOH + 100 mL H_2O solution for about 10 s at 6 volts, and the amount of sigma phase measured using computer software. Rockwell hardness tests in B or C scale (Ref 14), depending on hardness, were obtained from the larger samples. Vickers micro-hardness measurements were obtained from the smaller samples produced at the higher cooling rates, and the results converted to the corresponding Rockwell values.

4. Experimental Results

4.1 Analysis of CD3MN

Micrographs of CD3MN after cooling from 1100 °C to room temperature at various rates are shown in Fig. 2. The phase identification of δ, γ and σ is based on tint-etched color and EDS analyses (Ref 2, 3). Slower cooling rates, Fig. 2a, result in more σ-phase precipitation as expected. Figure 2d shows that σ-phase formation begins at the δ/γ grain boundaries and grows, consuming the δ matrix. The area percent of σ-phase, which is assumed to be approximately equal to the volume percent, was measured and is shown in Fig. 3. Since the kinetics of σ-phase transformation was reported to be very sluggish (Ref 3), σ-phase was not observed at the relatively fast cooling rates, 5 and 2 °C/min. The first measurable amounts of σ-phase were in the sample cooled at 0.5 °C/min, which was 0.54%. Therefore, the nose of initial the CCT curve indicating 1% formation should appear at a slightly slower rate than 0.5 °C/min.

The CCT diagram calculated for CD3MN using Eq 3 is shown in Fig. 3, with the parameters V_i, n_i, and k_i's at various temperature steps i taken from Ref 3. This plot was obtained by assuming a temperature decrease of 50 °C per step-wise cooling path (Fig. 1); Δt in Eq 3 was obtained by dividing the temperature step (i.e., 50 °C) by the cooling rate. The CCT diagram was then constructed by plotting the step-wise time duration, $t_{\text{step}} = (1100 - T_i)/\text{cooling rate}$ and the corresponding volume at step i, V_i versus the temperature T_i. It is noted that τ_i (Eq 2) is used for the calculation of V_i in Eq 3, but t_{step} is used for plotting the CCT curves in the temperature versus time field. This approach resulted in better agreement between

Table 1 Measured chemical composition of samples

	C	Mn	Si	P	S	Cr	Ni	Mo	Cu	W	N	Fe
CD3MN	0.029	0.60	0.65	0.025	0.022	22.1	5.45	2.98	0.22	0.063	0.15	Bal.
CD3MWCuN	0.034	0.59	0.87	0.023	0.011	24.5	7.33	3.62	0.67	0.76	0.23	Bal.

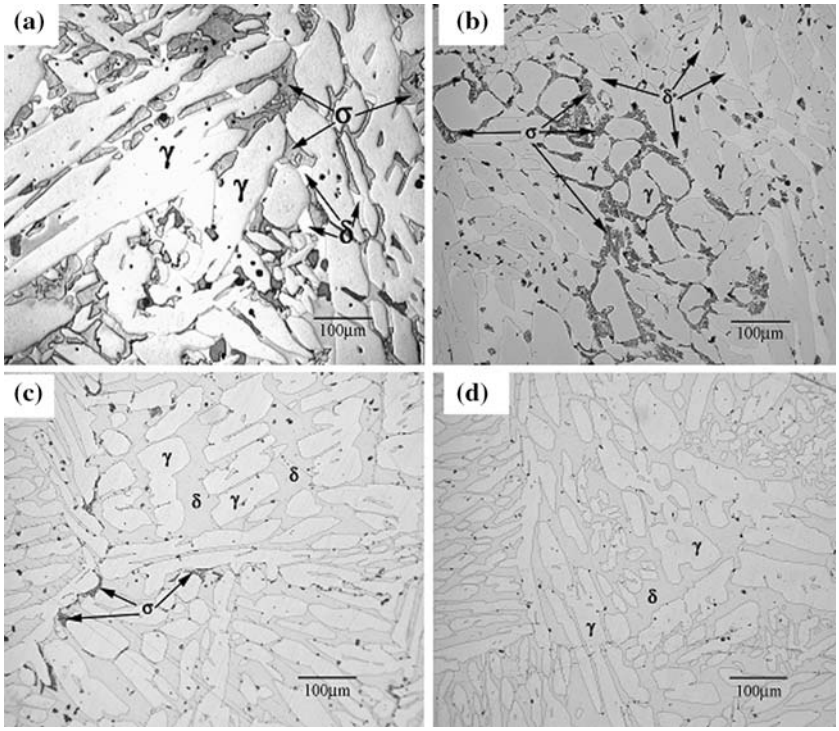

Fig. 2 Optical micrographs of CD3MN after continuous cooled at the rates of (a) 0.01, (b) 0.1, (c) 0.5, and (d) 1 °C/min

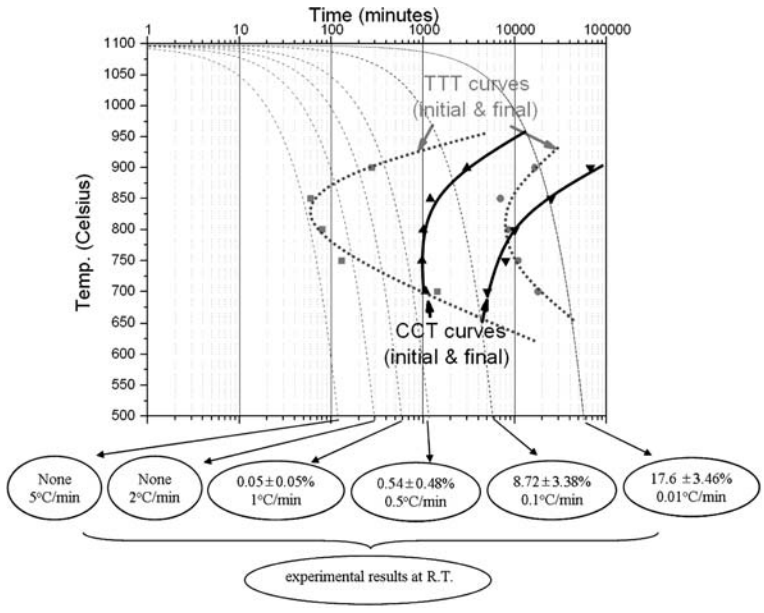

Fig. 3 Calculated CCT curves of CD3MN showing initial and final sigma phase precipitation superimposed on the corresponding TTT curves. Experimental results obtained when cooling from 1100 °C to room temperature are indicated in circles. Cooling rates were 5, 2, 1, 0.5, 0.1, 0.01 °C/min, shown respectively from left to right in the diagram

calculation and experimental observations than was observed by Wilson et al. (Ref 4, 12), who were forced to add a non-systematic time to match their calculated results to experimental data, since their calculated CCT diagram plotted $\tau_i + \Delta t$ versus T_i (Ref 12).

Observation of Fig. 3 shows the nose of the initial CCT curve for CD3MN is located between 750 and 800 °C at approximately 1000 min. This location is approximately an order of magnitude longer, and decreased in temperature by about 100 °C, from the initial TTT curve, which is included for comparison in Fig. 3.

4.2 Analysis of CD3MWCuN

Micrographs of CD3MWCuN after cooling from 1100 °C to room temperature at various rates are shown in Fig. 4. A $\sigma + \gamma_2$ eutectoid-type assemblage, identified based on SEM back-scattered electron (BSE) images coupled with energy dispersive spectroscopy (EDS) (Ref 3), was observed in the δ matrix. This observation agrees with reported results for Zeron 100, the wrought counterpart alloy of CD3MWCuN (Ref 15). The measured area percentages of σ-phase are shown in Fig. 5. The σ-phase transformation occurs more rapidly than in CD3MN due to higher Cr and Mo concentrations and different transformation mechanisms (i.e., the observed eutectoid-like morphology) (Ref 3). Thus, σ-phase was observed even at the relatively fast cooling rates of 5 and 2 °C/min. However, no σ-phase was seen in the extremely fast cooling rates produced using the Bridgman furnace. Therefore, the nose of initial CCT curve should be located at a cooling profile between 5 °C/min and that obtained with a 0.100 mm/s velocity with the Bridgman furnace.

The corresponding CCT curve for CD3MWCuN, determined in a manner analogous to that for CD3MN, is shown in Fig. 5. The nose of the CCT curve, which is shifted to lower temperatures and longer times, was calculated to be between 700 and 750 °C at a time of approximately 28 min.

4.3 Hardness Tests

The results of Rockwell hardness test for CD3MN and CD3MWCuN cooled at various rates are shown in Fig. 6 and 7, respectively. CD3MN remains steady at approximately 94.5

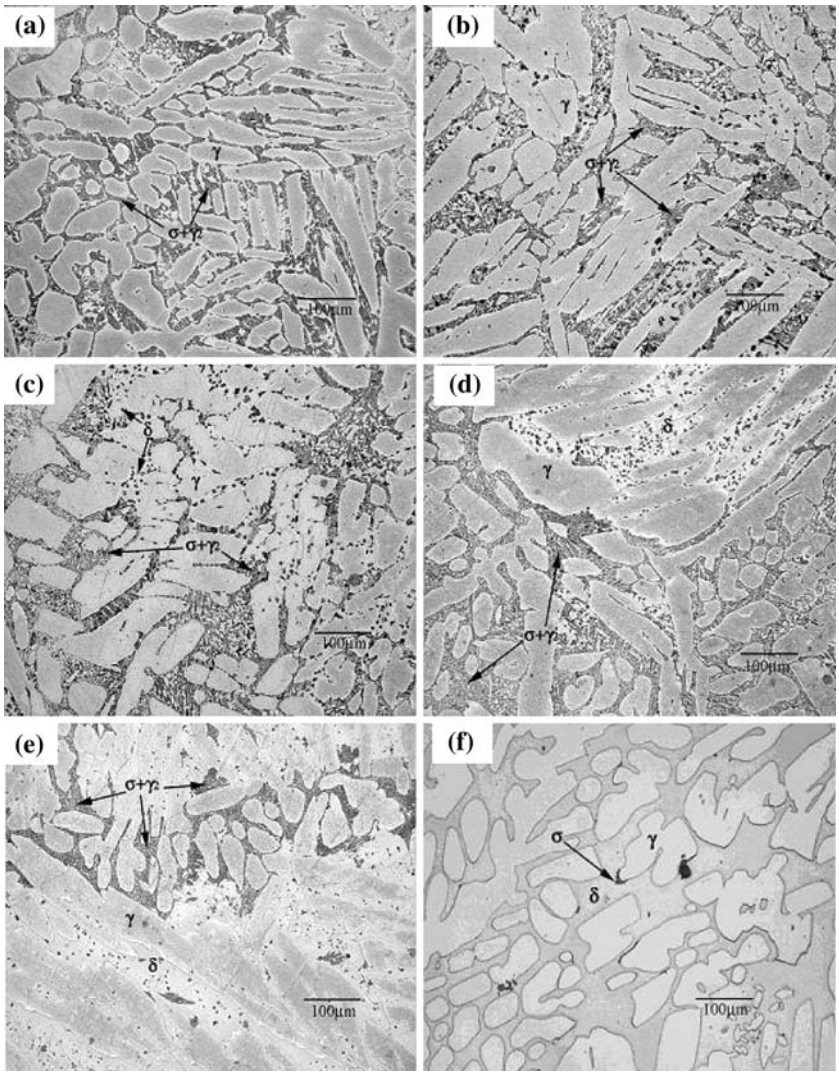

Fig. 4 Optical micrographs of CD3MWCuN after continuous cooled at the rates of (a) 0.1, (b) 0.5, (c) 1, (d) 2, (e) 5 °C/min and fast cooled using the Bridgman furnace with the velocity of 0.100 mm/s

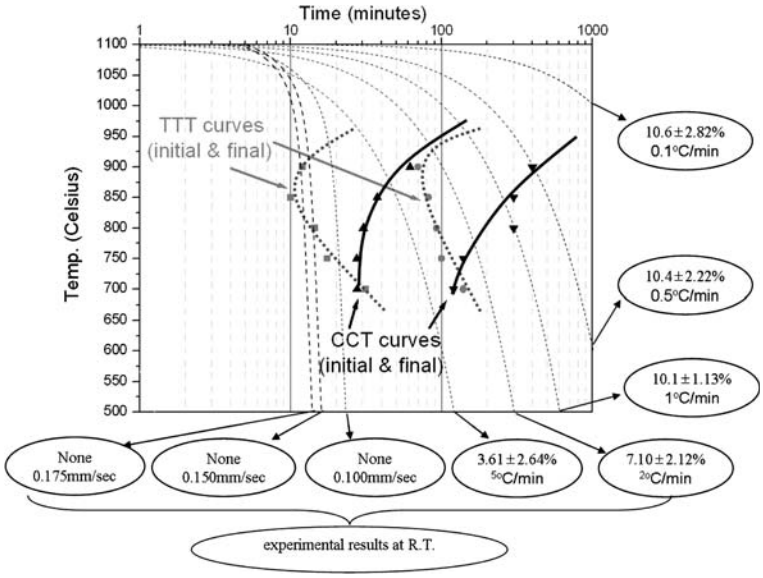

Fig. 5 Calculated CCT curves of CD3MWCuN showing initial and final sigma phase precipitation superimposed on the corresponding TTT curves. And experimental results cooling from 1100 °C to room temperature are indicated in circles. Cooling curves are 0.175, 0.150, 0.100 mm/s using the Bridgman furnace, and 5, 2, 1, 0.5, 0.1 °C/min using a tube furnace shown respectively from left to right in the diagram

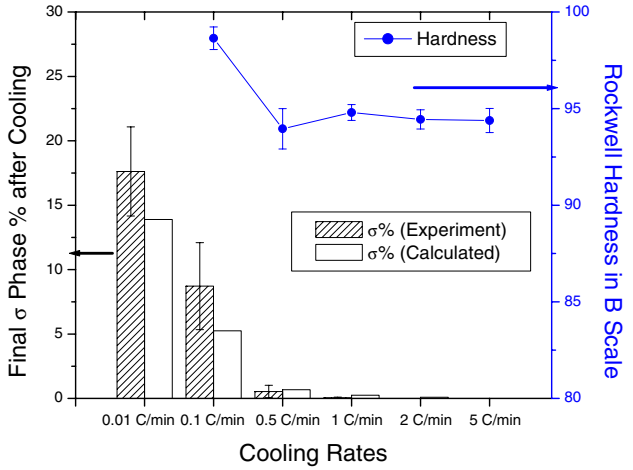

Fig. 6 Final σ phase percent after cooling at various rates and corresponding Rockwell B scale hardness measured for CD3MN

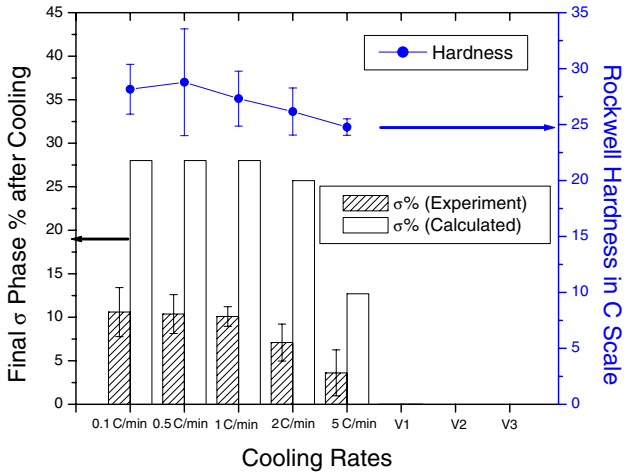

Fig. 7 Final σ phase percent after cooling at various rates and corresponding Rockwell B scale hardness measured for CD3MWCuN

Rockwell B until the volume percentage of sigma increases substantially at the 0.1 °C/min cooling rate. Hardness of CD3MWCuN is slightly higher initially than for CD3MN, being approximately 26 Rockwell C, and increases with increasing precipitation, which occurs at cooling rates as high as 5 °C/min. The hardness for CD3MWCuN ranges between 26 and 30 Rockwell C.

5. Discussion

Observation of Fig 3 and 5 show that the calculated CCT curves for both CD3MN and CD3MWCuN are shifted to lower temperatures and longer times than the previously determined TTT curves. This phenomenon is commonly observed, since the driving force for precipitation remains small near the TTT curve (Ref 16). The observed volume percentages of sigma as a function of imposed cooling rate are included within circles below the CCT diagrams of Fig 3 and 5. The calculated CCT diagrams agree well with the experimental results. For example, the initial curve of CD3MN (which corresponds to 1% sigma precipitation) is located at a somewhat slower time than expected given a 0.5 °C/min cooling path. The amount of σ-phase measured at this cooling rate is 0.54%. Similar agreement is found for CD3MWCuN, although the position of the nose for this sample is somewhat less exact. All of the cooling rates obtained using the Bridgman furnace were too rapid to intersect the nose of the calculated CCT curve, and no precipitation was seen experimentally. The fastest cooling rate obtained with the conventional furnace (5 °C/min) falls well within the CCT curve, and a considerable amount of precipitate was measured (3.61% ± 2.64%).

Figure 6 and 7 show the comparison between experiment and derived σ-phase percent after cooling in CD3MN and CD3MWCuN, respectively. The program Thermo-Calc was used to determine the calculated equilibrium amounts. The kinetically slower transforming CD3MN system (Fig. 6) shows reasonable agreement between experiment and derived, well within experimental error. However, the kinetically faster transforming CD3MWCuN system (Fig. 7) shows poor agreement of calculation with experiment, presumably due to an overriding influence of kinetic factors and the observed dual-phase morphology of σ-phase formation. Since σ-phase starts to nucleate and grow along the grain boundaries between δ and γ, grain size could also be affecting the transformation kinetics during cooling. Such effects have been observed and discussed in other work (Ref 17).

The results of this study compare favorably to σ-phase precipitation behavior seen during continuous cooling of SAF 2205 DSS, the wrought counterpart alloy of CD3MN, where Chen and Yang (Ref 18) reported 1 volume percent σ-phase precipitation is achieved is observed at a cooling rate equivalent to 15 °C/min. The slightly slower rate of 0.5 °C/min is in agreement with previous results (Ref 3) that showed σ-phase transformation kinetics is more sluggish in cast duplex alloys than the wrought counterpart alloys, presumably due to grain size effects.

The results of hardness measurements are shown in Fig. 6 and 7 for CD3MN and CD3MWCuN, respectively. The measured hardness of the two alloys appears to follow σ-phase formation, with hardness increasing once the amount of σ-phase reaches approximately 5%. This phenomenon is in agreement with previous studies (Ref 1, 19).

6. Conclusions

The CCT diagrams of cast duplex stainless steels CD3MN and CD3MWCuN have been determined mathematically and experimentally. The calculated curves match well with the experimental results, with the nose of the curves being between 750-800 °C for 1000 min for CD3MN and 700-750 °C for 25 min for CD3MWCuN. For CD3MN, this is slightly delayed from the times reported for the wrought counterpart, SAF 2205. Equilibrium amounts of precipitation were found to be in agreement with Thermo-Calc predictions for CD3MN, but substantially lower for CD3MWCuN. This is believed due to the difference in formation kinetics, as evidenced by the varying morphology of the sigma in the two alloys. Hardness values were shown to increase when total volume percentage of precipitation reached approximately 5%, in agreement with previous reports.

Acknowledgments

This work was funded by the US Department of Energy (USDOE) through a subcontract with the University of Alabama at Birmingham, and was in collaboration with the Steel Founders' Society of America (SFSA) and their members. The authors are especially grateful to Eric Johnson and the John Deere Technology Center, Moline, Illinois, Keokuk Steel Castings, Keokuk, Iowa, and Stainless Foundry and Engineering, Inc., Milwaukee, Wisconsin for technical assistance, samples and access to their facilities.

References

1. J. Charles, The Duplex Stainless Steels: Materials to Meet Your Needs, *Proc. Conf. Duplex Stainless Steels'91*, vol. 1, Beaune, Les Editions de Physique, (Beaune, Physics Editions) 1991, p 3–48, in French
2. E.M. Johnson, Y.-J. Kim, L.S. Chumbley, and B. Gleeson, Initial Phase Transformation Diagram Determination for the CD3MN Cast Duplex Stainless Steel, *Scripta. Mater.*, 2004, **50**, p 1351–1354
3. Y.-J. Kim, L.S. Chumbley, and B. Gleeson, Determination of Isothermal Transformation Diagrams for Sigma-Phase Formation in Cast Duplex Stainless Steels, *Metall. Trans. A*, 2004, **35A**, p 3377–3386
4. B. Josefsson, J.-O. Nilsson, and A. Wilson, Phase Transformations in Duplex Steels and the Relation between Continuous Cooling and Isothermal Heat Treatment, *Duplex Stainless Steels'91,* vol. 1, J. Charles and S. Bernhardsson, Eds. (Beaune, France), Les Editions de Physique, 1991, p 67–75
5. A.Z. Hanzaki, R. Pandi, P.D. Hodgson, and S. Yue, Continuous Cooling Deformation Testing of Steels, *Metall. Trans. A*, 1993, **24A**, p 2657–2665
6. D.Q. Bai, S. Yue, T.M. Maccagno, and J.J. Jonas, Continuous Cooling Transformation Temperatures Determined by Compression Tests in Low Carbon Bainitic Grades, *Metall. Trans. A*, 1998, **29A**, p 989–1001
7. A.B. Cota, P.J. Modenesi, R. Barbosa, and D.B. Santos, Determination of CCT Diagrams by Thermal Analysis of an HSLA Bainitic Steel Submitted to Thermomechanical Treatment, *Scripta. Mater.*, 1999, **40**, p 165–169
8. M. Venkatraman, O.N. Mohanty, and R.N. Ghosh, Modeling of Transformation Kinetics in HSLA 100 Steel during continuous cooling, *Scand. J. Metall.*, 2001, **30**, p 8–13
9. M. Avrami, Kinetics of Phase Change II Transformation—Time Relations for Random Distribution of Nuclei, *J. Chem. Phys.*, 1940, **8**, p 212–224
10. E. Scheil, Starting Time of the Austenite Transformation, *Arch. Eisenhüttenwes.*, 1935, **12**, p 565–567
11. J.W. Cahnm, Transformation Kinetics During Continuous Cooling, *Acta Metall.*, 1956, **4**, p 572–575
12. A. Wilson and J.-O. Nilsson, Modelling the CCT-Diagram of Intermetallic Phase Formation in DSS from Isothermal Experiments, *Scand. J. Metall.*, 1996, **25**, p 178–185
13. J.S. Ye, H.B. Chang, and T.Y. Hsu, On the Application of the Additivity Rule in Pearlite Transformation in Low Alloy Steels, *Metall. Trans. A*, 2003, **34A**, p 1259–1264
14. G.E. Dieter, *Mechanical Metallurgy.* McGraw-Hill, London, United Kingdom, 1988
15. X.G. Wang, D. Dumortier, and Y. Riquier, Structural Evolution Of Zeron 100 Duplex Stainless Steel between 550 and 1100 °C, *Duplex stainless steels'91,* vol. 1, J. Charles and S. Bernhardsson Eds. (Beaune, France) Les Editions de Physique, 1991, p 127–134
16. D.A. Porter and K.E. Easterling, *Phase Transformations in Metals and Alloys*. 2nd ed., Chapman and Hall, London, United Kingdom, 1992
17. P.C. Campbell, E.B. Hawbolt, and J.K. Brimacombe, Microstructural Engineering Applied to the Controlled Cooling of Steel Wirerod: Part 3: Mathematical Model-Formaulation and Predictions, *Metall. Trans. A*, 1991, **22A**, p 2791–2805
18. T.H. Chen and J.R. Yang, Effects of Solution Treatment and Continuous Cooling on Sigma-Phase Precipitation in a 2205 Duplex Stainless Steel, *Mater. Sci. Eng. A*, 2002, **A311**, p 28–41
19. J.O. Nilsson, P. Kangas, T. Karlsson, and Q. Wilson, Mechancial Properties, Microstructural Stability and Kinetics of Sigma-Phase Formation in 29Cr-6Ni-2Mo-0,38N Superduplex Stainless Steel, *Metall. Trans. A*, 2001, **31A**, p 35–45